

**ORIGINAL
RESEARCH**

J.L. Boxerman
K.M. Schmainda
R.M. Weisskoff

Relative Cerebral Blood Volume Maps Corrected for Contrast Agent Extravasation Significantly Correlate with Glioma Tumor Grade, Whereas Uncorrected Maps Do Not

BACKGROUND AND PURPOSE: Relative cerebral blood volume (rCBV) estimates for high-grade gliomas computed with dynamic susceptibility contrast MR imaging are artificially lowered by contrast extravasation through a disrupted blood-brain barrier. We hypothesized that rCBV corrected for agent leakage would correlate significantly with histopathologic tumor grade, whereas uncorrected rCBV would not.

METHODS: We performed dynamic T2*-weighted perfusion MR imaging on 43 patients with a cerebral glioma after prebolus gadolinium diethylene triamine penta-acetic acid administration to diminish competing extravasation-induced T1 effects. The rCBV was computed from non-necrotic enhancing tumor regions by integrating the relaxivity-time data, with and without contrast extravasation correction by using a linear fitting algorithm, and was normalized to contralateral brain. We determined the statistical correlation between corrected and uncorrected normalized rCBV and histopathologic tumor grade with the Spearman rank correlation test.

RESULTS: Eleven, 9, and 23 patients had WHO grades II, III, and IV glioma, respectively. Mean uncorrected normalized rCBVs were 1.53, 2.51, and 2.14 (grade II, III, and IV). Corrected normalized rCBVs were 1.52, 2.84, and 3.96. Mean absolute discrepancies between uncorrected and corrected rCBVs were 2% (0%–15%), 16% (0%–106%), and 74% (0%–411%). The correlation between corrected rCBV and tumor grade was significant (0.60; $P < .0001$), whereas it was not for uncorrected rCBV (0.15; $P = .35$).

CONCLUSION: For gliomas, rCBV estimation that correlates significantly with WHO tumor grade necessitates contrast extravasation correction. Without correction, artificially lowered rCBV may be construed erroneously to reflect lower tumor grade.

The appropriate management of newly identified brain tumors suspected to be of glial origin currently requires invasive biopsy, because the prognoses and treatments for benign, low-grade, and high-grade lesions differ greatly. MR perfusion imaging may provide a noninvasive diagnostic tool for properly grading lesions, as well as identifying the most malignant region of a tumor for guiding stereotactic biopsy, and monitoring response to therapy that may precede conventionally assessed changes in tumor morphology and enhancement characteristics. Relative cerebral blood volume (rCBV) has been the most widely used parameter derived from dynamic susceptibility contrast (DSC) perfusion MR imaging for predicting brain tumor grade,^{1–8} although other parameters, such as relative recirculation,⁹ vascular permeability,¹⁰ and blood flow,⁸ have also been investigated. rCBV has been shown to correlate positively with choline (a marker of prolif-

erative tumor activity),¹¹ to correspondingly increase with evolution of a low-grade to high-grade glioma,¹² and to correlate with glucose uptake and tumor angiogenesis in human gliomas.¹³ In addition, rCBV may help differentiate primary central nervous system (CNS) lymphoma and glioblastoma multiforme (GBM)¹⁴ and certain metastases from high-grade astrocytomas,¹⁵ aid in the differentiation of posttreatment changes from tumor recurrence^{16,17} and predict early local recurrence or malignant transformation.¹⁸

It is generally agreed that microvascular blood volume is elevated in tumors, with an association between microvascular density and tumor energy metabolism,¹³ and with a clear correlation between increased tumor neovascularity (irregular, enlarged, and distorted microvessels) and malignancy.^{19,20} Nonetheless, the literature has been inconsistent concerning the correlation between MR rCBV and histologic tumor grade. For example, previous studies have demonstrated no correlation between rCBV and low- versus high-grade gliomas²¹ and no statistical difference in rCBV between grade I and II, grade II and III, and grade III and IV gliomas.³ Other studies, however, have found the opposite to be true, including positive correlation between rCBV and low- versus high-grade gliomas^{5,8,9,13} and significantly different rCBV between grade II, grade III, and grade IV gliomas.⁷ The disparity of these findings suggests that careful attention must be paid to the rCBV computation process, and one point of differing methodology involves contamination of derived concentration-time data by contrast agent extravasation.

When confined to the intravascular space, paramagnetic

Received June 30, 2005; accepted after revision September 1.

From the Department of Radiology (J.L.B.), Rhode Island Hospital and Brown University Medical School, Providence, RI; the Department of Biophysics (K.M.S.), Medical College of Wisconsin, Milwaukee, Wis; and the Massachusetts General Hospital NMR Center (R.M.W.), Charlestown, Mass.

Current affiliation for R.M.W.: Fidelity Biosciences, Watertown, Mass.

Supported in part by National Institutes of Health grants R01-HL39810 (to R.M.W.), MD1-RR00058 (to K.M.S.), and R01-CA082500 (to K.M.S.) and the Medical College of Wisconsin Cancer Center (to K.M.S.).

Presented in part at the 42nd Annual Meeting of the American Society of Neuroradiology, Seattle, Washington, 2004, and at the 2nd Annual Meeting of the Society of Magnetic Resonance, San Francisco, Calif, 1994.

Address correspondence to Jerrold L. Boxerman, MD, PhD, Department of Radiology, Rhode Island Hospital, Brown University School of Medicine, 593 Eddy Street, Providence, RI 02903.

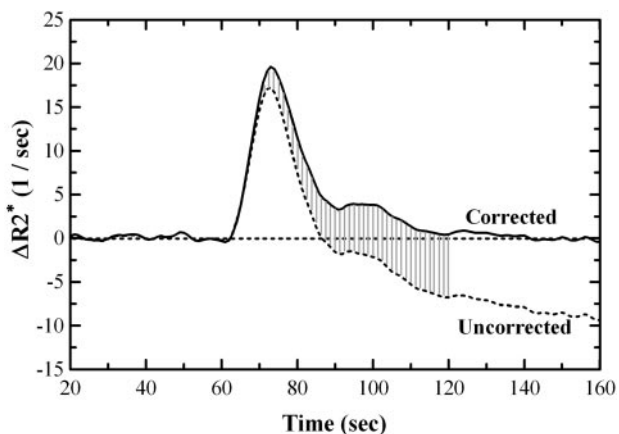


Fig 1. Typical corrected and uncorrected $\Delta R2^*$ curves are shown. Note that even the first-pass curve is shifted to account for early leakage occurring during this segment. Without correction, the area under the curve (relative cerebral blood volume [rCBV]) is underestimated, even for integration techniques that stop at zero crossing or use gamma fitting.

contrast agents (eg, gadolinium-diethylene-triaminepentaacetic acid [Gd-DTPA]) produce signal intensity loss in the extravascular space on T2-weighted scans,²² and susceptibility contrast-based rCBV maps are computed by integrating the resulting transverse relaxivity changes ($\Delta R2$) that occur over a dynamic first-pass injection.^{23,24} However, because Gd-DTPA is also an effective T1 relaxation enhancer, the susceptibility-contrast signal intensity loss can be masked by signal intensity increase in regions where T1 effects are significant. This occurs in enhancing tumors, where Gd-DTPA extravasates into the interstitial space of lesions with significant blood-brain barrier breakdown. In such instances, rCBV will be underestimated, which may affect tumor grade prediction. Although both nonlinear γ -fitting and numerical integration to the peak of the first-pass $\Delta R2$ curve can reduce this effect by focusing on the early first-pass, the entire first-pass curve is in principle contaminated by the T1 effect, necessitating global curve correction for accurate rCBV estimates (Fig 1). To the best of our knowledge, besides a preliminary study performed by Donahue et al,⁵ there has been no formal comparison documenting the role of contrast agent leakage correction in the rCBV map process.

The purpose of this study was to determine whether T1 contamination from contrast agent extravasation significantly affects predicted tumor grade based upon dynamic susceptibility contrast MR rCBV estimates. Because we assume that rCBV should correlate significantly with tumor grade, differences in significance of correlation between rCBV with and without extravasation correction and tumor grade should reflect the impact of leakage correction on rCBV accuracy. To this end, we derived a robust strategy for approximately correcting the T1 enhancement effect. This strategy uses linear fitting to estimate the T1 contamination due to agent extravasation and, by removing the leakage term, allows generation of both corrected rCBV maps and first-order estimates of vascular permeability. We applied this technique to human brain tumor data and hypothesized that rCBV corrected for contrast agent leakage would correlate significantly with histopathologic tumor grade, whereas uncorrected rCBV would not.

Methods

Patient Selection

Patients with a cerebral glioma on prior imaging studies or a history of a biopsy-confirmed or suspected cerebral glioma and who were referred for conventional cerebral contrast-enhanced MR imaging, were recruited for additional perfusion MR imaging. Patients who refused the additional rCBV examination, or were unable to remain still during the entirety of the MR imaging examination, were excluded. All patients who underwent rCBV mapping gave informed written consent under guidelines approved by the Institutional Review Board at the Medical College of Wisconsin. Studies were excluded if (1) a tissue diagnosis was not available, or biopsy did not support a diagnosis of a glioma; (2) it was a follow-up examination (only one rCBV study per patient is included); or (3) data were corrupted by patient motion or technical error that precluded postprocessing. Tumors were classified and graded according to the World Health Organization 1993 classification.²⁵

Imaging

MR imaging was performed on a 1.5T whole-body scanner (Signa; GE Medical Systems, Milwaukee, Wis) fitted with a 12-in local 3-axis gradient coil and a quadrature transmit-receive bird cage radio-frequency coil (IGC-Medical Advances, Milwaukee, Wis). Conventional precontrast T1-weighted images were acquired (spin-echo [SE]; echo time [TE]/repetition time [TR] = 11 ms/500 ms; matrix = 256 × 256; number of excitations = 2; 5 mm/1.5 mm). Immediately before dynamic imaging, a 0.05 to 0.10-mmol/kg prebolus dose of gadodiamide (Omniscan; GE Healthcare, Princeton, NJ) was administered to diminish T1 effects that might result from agent extravasation.^{5,26} (If the initial tissue T1 is decreased with prebolus contrast agent, subsequent T1-induced signal intensity changes, which might occur from extravasation during the first-pass study, are thereby reduced. Furthermore, leakage of the prebolus dose in areas of blood-brain barrier disruption may diminish the intravascular-extravascular concentration gradient driving extravasation during bolus passage.) Single-shot gradient-echo (GE) echo-planar images were acquired for 1 minute before and 2 minutes after a 0.15- to 0.25-mmol/kg bolus injection of Gd-DTPA injected at 3 to 5 mL/s. Five 5-mm sections, with an interslice spacing of 1.5 mm, were acquired with fat suppression (TE = 30 ms; TR = 1 second; field of view = 24 × 24 cm; image matrix = 64 × 64). Subsequently, conventional postcontrast T1-weighted images were acquired with the same imaging parameters as the precontrast acquisition.

Map Generation and Data Analysis

For each voxel, the dynamic signal intensity curve $S(t)$ was converted to a relaxivity-time curve ($\Delta R2^*(t) = -(1/TE)\ln(S(t)/S_0)$), a parameter related to the concentration of gadolinium in the voxel. The typical uncorrected rCBV is estimated by integrating the relaxivity-time curve. To make a correction to this estimate for contrast agent leakage, as shown in greater detail in the Appendix, the measured relaxivity change for each voxel can be approximated as a linear combination of whole-brain average $\overline{\Delta R2^*(t)}$ in nonenhancing voxels, $\overline{\Delta R2^*(t)}$, and its time integral,

$$1) \quad \Delta R2^*(t) \approx K_1 \overline{\Delta R2^*(t)} - K_2 \int_0^t \overline{\Delta R2^*(t')} dt'$$

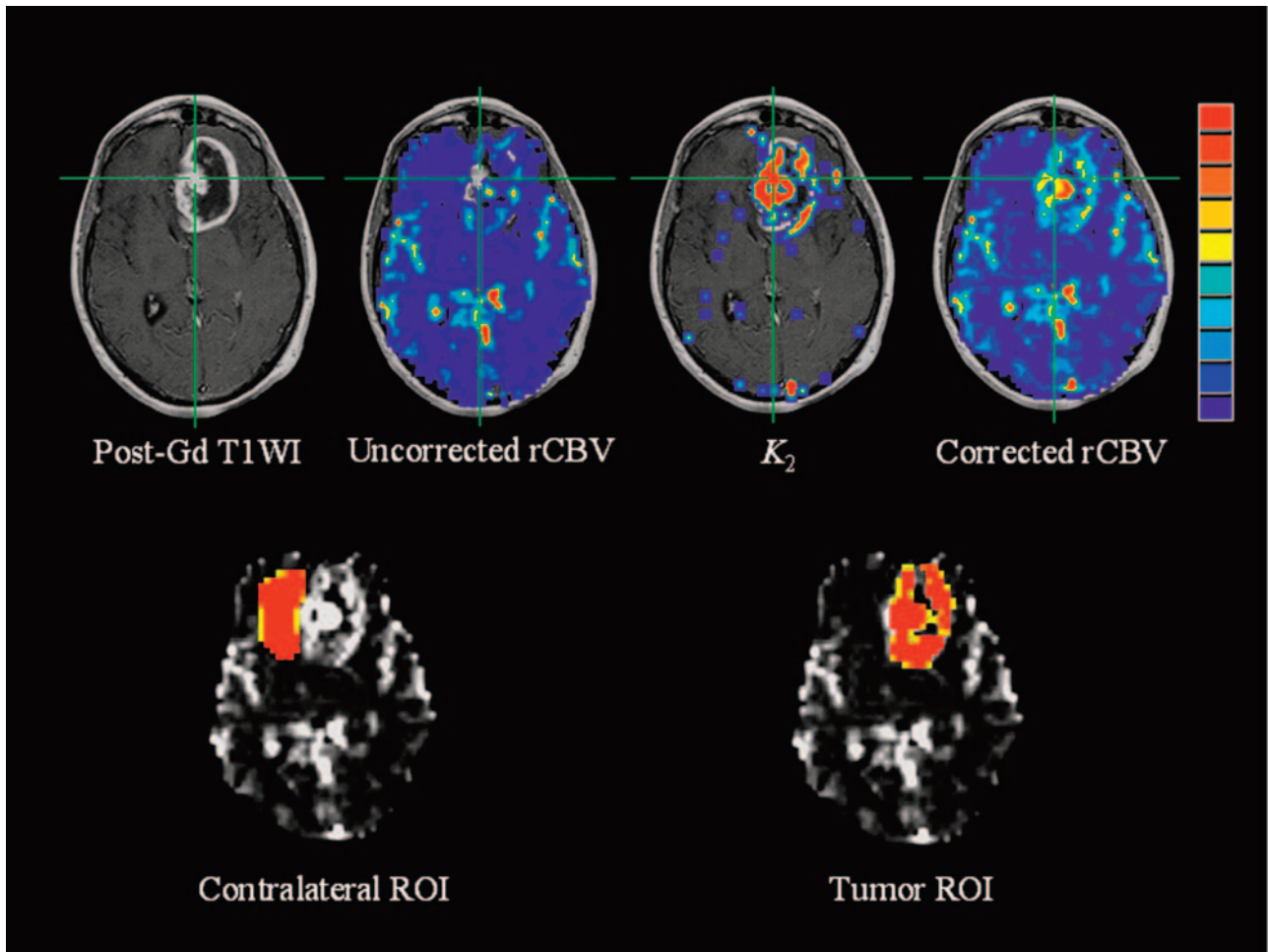


Fig 2. Typical case (grade IV glioma) demonstrating post-Gd T1, uncorrected relative cerebral blood volume (rCBV) map with artificially low tumor blood volume, the K_2 parameter map from our fitting algorithm showing areas of greatest correction, and the corrected rCBV map highlighting a focus of corrected very high blood volume. On the bottom are sample tumor and normal brain regions of interest based on the corrected rCBV map.

where $K_1 \cdot \overline{\Delta R2^*}(t)$ reflects the uncontaminated $\Delta R2^*(t)$ for each pixel, and the K_2 term reflects the effects of leakage. It then follows that rCBV corrected for leakage is simply derived from contaminated rCBV and $\overline{\Delta R2^*}(t)$.

$$2) \quad rCBV_{corr} = rCBV + K_2 \int_0^T dt'' \int_0^{t''} \overline{\Delta R2^*}(t') dt'$$

The effect of leakage on the CBV estimate for each voxel is removed by adding the estimate of K_2 (which varies by pixel) times $\int_0^T dt'' \int_0^{t''} \overline{\Delta R2^*}(t') dt'$ (which is the same for all pixels) to the uncorrected CBV estimate.

To implement the correction scheme, we first computed a whole-brain mask for each slice in each dataset, consisting of those voxels with average baseline signal intensity (mean of the first 60 acquired time points) exceeding 20 SDs of background noise. We next estimated $\overline{\Delta R2^*}(t)$ by averaging $\Delta R2^*(t)$ for all pixels within the mask that did not demonstrate signal intensity enhancement (averaged over the final 10 time points) greater than 1 SD above that pixel's average baseline and estimated $\int_0^t \overline{\Delta R2^*}(t') dt'$ by using trapezoidal integration over the 120 acquired time points (Fig 1). $\overline{\Delta R2^*}(t)$ and $\int_0^t \overline{\Delta R2^*}(t') dt'$ are functions of time only, not space. For each pixel within the mask, we determined K_1 and K_2 by using a linear least-squares fit to Equation (1). We computed 4 maps: uncorrected rCBV

(trapezoidal integration of $\overline{\Delta R2^*}(t)$), corrected rCBV (Equation [2]), and the least-squares coefficients, K_1 and K_2 . All map generation and data processing were performed by using the AFNI (Analysis of Functional Neuroimages) platform.²⁷ An example of maps generated for a typical grade IV glioma is illustrated in Fig 2.

Average uncorrected and corrected rCBVs for each glioma were then computed from the appropriate maps within an identical region of interest derived from the corrected rCBV maps. Specifically, the regions of interest included areas of increased rCBV. In the cases where there was no apparent increased rCBV, which can often occur with lower-grade tumors, the regions of interest encompassed areas of enhancement apparent on the postcontrast T1-weighted images. The regions of interest did not include areas of necrosis or nontumor macrovessels evident on postcontrast T1-weighted images (Fig 2). Each average rCBV estimate was then normalized to average rCBV in a similar-sized region of interest in the contralateral (normal) brain white matter. The percentage difference between corrected and uncorrected rCBV for each tumor was computed (magnitude of difference divided by mean) and averaged across each tumor grade. The statistical correlation between the normalized tumor rCBV (both corrected and uncorrected) and histopathologic tumor grade was determined with the Spearman rank correlation test, by using $P = .05$ as the significance threshold.

Patient histology and imaging results, grouped by tumor grade			
Patient No./ Age (y)/Sex	Pathologic Diagnosis	Corrected rCBV	Uncorrected rCBV
Grade II			
1/80/M	Ependymoma	2.18	2.18
2/50/M	Low-grade glioma	1.56	1.56
3/59/M	Oligodendroglioma	1.46	1.46
4/39/M	Oligodendroglioma	0.72	0.72
5/50/M	Astrocytoma	1.39	1.20
6/53/M	Astrocytoma	1.35	1.35
7/66/F	Astrocytoma	3.35	3.08
8/19/M	Astrocytoma	0.44	0.44
9/48/F	Astrocytoma	1.61	1.61
10/23/F	Central neurocytoma	2.33	2.33
11/30/M	Mixed glioma	0.62	0.62
Grade III			
1/40/F	Anaplastic astrocytoma	3.44	3.47
2/32/F	Anaplastic astrocytoma	0.74	0.74
3/37/F	Anaplastic astrocytoma	5.63	5.55
4/47/M	Anaplastic astrocytoma	4.28	1.31
5/77/M	Anaplastic astrocytoma	2.42	2.82
6/50/M	Anaplastic astrocytoma	2.02	1.68
7/41/M	Anaplastic astrocytoma	2.18	2.18
8/55/M	Anaplastic oligodendroglioma	2.25	2.25
9/41/M	Anaplastic oligodendroglioma	2.63	2.63
Grade IV			
1/50/M	GBM	1.65	1.65
2/52/F	GBM	3.35	1.06
3/73/M	GBM	4.92	4.85
4/69/M	GBM	11.03	-0.41
5/48/M	GBM	9.18	0.15
6/68/M	GBM	5.56	5.56
7/50/F	GBM	4.16	2.09
8/42/M	GBM	3.33	1.87
9/74/M	GBM	3.91	0.44
10/49/F	GBM	2.98	2.98
11/71/F	GBM	4.23	4.21
12/30/M	GBM	2.97	2.86
13/41/M	GBM	2.59	-0.39
14/65/F	GBM	3.82	2.73
15/42/M	GBM	2.59	2.51
16/66/M	GBM	4.10	4.08
17/56/M	GBM	1.70	1.06
18/77/M	GBM	4.28	4.28
19/54/F	GBM	2.13	1.63
20/55/M	GBM	5.51	1.85
21/45/M	GBM	1.71	-0.59
22/45/F	Anaplastic oligodendroglioma	2.22	2.17
23/66/M	Mixed GBM + low-grade astrocytoma	3.07	2.59

Note.—rCBV indicates relative cerebral blood volume; GBM, glioblastoma multiforme.

Results

A total of 43 patients were suitable for evaluation, consisting of 30 men and 13 women, with mean age of 52 years and an age range of 19 to 80 years. Table 1 lists the age, sex, and histopathologic diagnosis for all patients studied. Eleven, 9, and 23 patients had tumors classified as WHO grades II, III, and IV, respectively. The grade II tumors included ependymoma ($n = 1$), astrocytoma ($n = 5$), oligodendroglioma ($n = 2$), low-grade or mixed glioma ($n = 2$), and neurocytoma ($n = 1$). The grade III tumors included anaplastic astrocytoma ($n = 7$) and anaplastic oligodendrogliomas ($n = 2$). The grade IV tumors included both de novo and recurrent GBM ($n = 22$) and

anaplastic oligodendroglioma ($n = 1$). For the astrocytomas, a 4-tiered system was applied, but no grade I lesions were included in this series. The oligodendroglial subtypes were graded with a similar 4-tiered system, and one oligodendroglial tumor was indeed graded IV, demonstrating all the features of a GBM but with a strong preponderance of oligodendroglial neoplastic cells. The ependymoma in our series was a grade II lesion. It demonstrated some foci of necrosis and mitoses, but this was felt not to be necessarily indicative of malignancy.

Uncorrected normalized rCBVs (mean \pm SD) for grades II, III, and IV were 1.53 ± 0.85 , 2.51 ± 1.40 , and 2.14 ± 1.70 , respectively. Corrected normalized rCBVs were 1.52 ± 0.79 , 2.84 ± 1.43 , and 3.96 ± 2.26 . These data are summarized in Fig 3. The percentage differences between uncorrected and corrected rCBVs (mean [range]) were 2% (0%–15%), 16% (0%–106%), and 74% (0%–411%) for grades II, III, and IV, respectively. The Spearman rank correlation coefficient between corrected rCBV and tumor grade was 0.60, which demonstrates significant correlation ($P < .0001$). By comparison, uncorrected rCBV and tumor grade were not significantly correlated, with a Spearman rank correlation coefficient of 0.15 ($P = .35$).

Figure 4 compares the percentage difference between corrected and uncorrected rCBV for each of the 43 gliomas, separated by grade. For all 3 grades, there were several cases where correction made no difference (shown in gray), probably because of a combination of low vascular permeability and the Gd preload. Most of the high-grade tumors, however, had >10% difference, with 6 cases differing by more than a factor of 2.

Discussion

We describe a robust and extremely time-efficient fitting strategy for approximately removing the T1 enhancement effect that artifactually diminishes estimated rCBV and demonstrate that corrected rCBV correlates significantly with glioma tumor grade whereas uncorrected rCBV does not. Our correction strategy uses linear fitting to estimate the T1 contamination caused by agent extravasation and, by removing most of the effects of the leakage term, allows generation of both corrected rCBV maps and first-order estimates of vascular permeability. The technique improves the reliability of rCBV mapping for several reasons.

First, the technique moderates the effects of contrast agent extravasation on T2*-weighted signal intensity loss. The extravasated contrast agent relaxes extravascular, extracellular protons and thus increases signal intensity, competing against and corrupting the susceptibility contrast-induced signal intensity drop used to estimate tumor hemodynamics. In addition to contamination by competing T1 effects, extravasation of agent into the extravascular, extracellular space would also be expected to diminish $\Delta R_2(t)$ by decreasing the magnetization difference between the intravascular and extravascular spaces ($\Delta\chi$), and hence the degree of susceptibility effect. Although the model derivation shown in the Appendix does not explicitly take this effect into account, in theory it would be modeled with an expression that looks very similar to Equation (A6), and thus we would expect a decrease in ΔR_2 approximately proportional to $C_T(t)$. Thus, the CBV correction

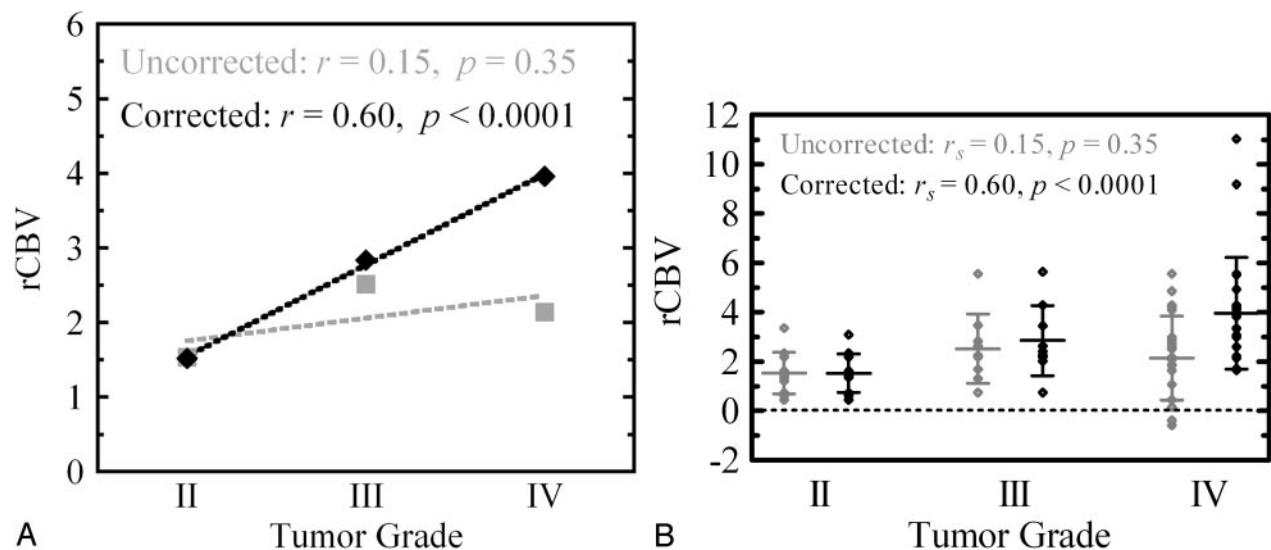


Fig 3. A, rCBV estimates corrected for contrast agent extravasation correlate significantly with glioma grade by using a Spearman rank correlation, whereas uncorrected relative cerebral blood volume (rCBV) does not. The disparity is due primarily to artificially low uncorrected blood-volume estimates in high-grade tumors that arises from the competing T1 effects of Gd leaking through disrupted blood-brain barrier.

B, Despite significant correlation, there exists moderate corrected rCBV variability within each grade and intergrade overlap. This supports the notion that glioma grading remains controversial and that multiple parameters, including vascular permeability and vessel size distribution, will probably be required in aggregate for accurate prognostication.

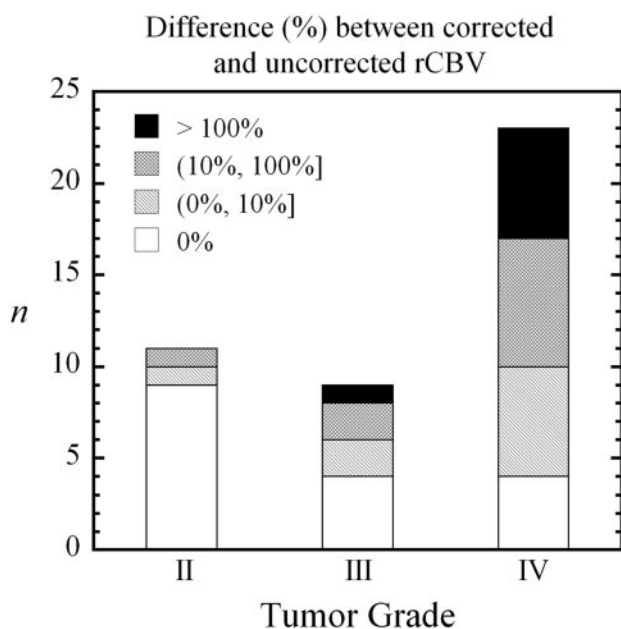


Fig 4. Percentage difference between corrected and uncorrected relative cerebral blood volume (rCBV) for each of the 43 gliomas separated by grade. For all 3 grades, there were several cases in which correction made no difference (shown in white), probably because of a combination of low vascular permeability (possibly from steroids) and the Gd preload. Most of the high-grade tumors, however, had >10% difference, with 6 cases differing by at least a factor of 2.

should remain robust in the presence of this effect, and, while K_2 should still be proportional to the leakage (PS), the quantitative interpretation of K_2 would become more complex.

Second, the fitting-correction technique extends the observation time that can be practically used in the dynamic phase of the contrast bolus, which potentially increases the signal intensity-to-noise ratio of the computed rCBV maps. Several techniques have been described in the literature for handling leakage contamination of rCBV estimates from dynamic sus-

ceptibility contrast MR imaging. γ -Variate-fitting techniques have been used to correct the tail deviation of $\Delta R2(t)$ caused by extravasation enhancement (eg,^{2,6,8}), which for whole-curve numerical integration would artificially lower rCBV estimates; however, the entire $\Delta R2(t)$ curve is reduced in absolute amplitude because contrast extravasates throughout the bolus, not just at the tail, and hence elimination of only the tail contamination is theoretically insufficient. Early bolus extravasation would be greater for high-grade tumors with high vascular permeability, and ignoring this effect could yield large percentage error in high-grade tumors. In addition, the γ -variate fit is nonlinear and has been found to be often unstable and potentially time-consuming in practice, with small variations in the initial parameter estimates yielding wide variations in the results, even with data averaged over regions of interest in areas of high perfusion.²⁸ We propose that, should γ -variate fitting be desired (which actually generates lower CBV map signal intensity-to-noise ratio [SNR] than numerical integration,²⁴), it be applied to the corrected data to eliminate the recirculation peak.

Similarly, some published techniques consider only the peak $\Delta R2$ or integrate from the beginning of the bolus to the peak $\Delta R2$ (“limited integration method”²⁹) to avoid late bolus T1 contamination, but this would also not account for artifactual $\Delta R2(t)$ suppression from early bolus extravasation and would not incorporate late bolus $\Delta R2$ effects into the rCBV estimate. Another published technique subtracts a “tilted” baseline drawn from the beginning to the end point of bolus from the bolus points to “pull up” $\Delta R2(t)$ (“baseline subtraction method”³⁰). This assumes that the tail of $\Delta R2(t)$ ideally matches the initial baseline and that there is homogeneous, linear contamination throughout the bolus. The technique described herein approximately corrects the entire $\Delta R2(t)$ curve by using a stable, linear fit, permitting numerical integration over the entire first pass and thereby realizes advantages in accuracy and map SNR (precision).

Besides the correction strategies discussed above, there are other alternatives. Double-echo T2*-weighted perfusion MR imaging has also been described, which uses a simple exponential model and signal intensities at 2 different TEs to compute $\Delta R2(t)$ without T1 contamination.³¹⁻³³ A GE planar imaging (EPI) sequence with small flip angle and long TR could also be used to reduce sensitivity to T1 contamination but at the expense of lower SNR and lower temporal resolution. Furthermore, the eventual approval of large molecular weight, intravascular susceptibility-based contrast agents (eg,³⁴) for clinical use may eliminate the need for correction entirely, although they may introduce practical issues with regard to conventional postcontrast imaging. A formal comparison of all correction techniques and their relative error, including the potential use of intravascular contrast agents, is beyond the scope of this report. Ultimately, direct histopathologic evaluation of microvessel volume in an animal model would be helpful to better understand the tradeoffs involved and the degree of correction that can be realized.

It is also worth considering whether K_1 in Equation (A9) could be used as the rCBV estimate itself. To the extent that the arterial bolus changes very slowly in time, so that the convolution in Equation (A1) simply becomes $\overline{C}_c(t) \approx C_a(t) \cdot \{F\int R(t)dt\} \approx C_a(t)V$, K_1 is exactly the blood volume. This condition does not necessarily hold early in the bolus. As a correction term, however, the distinction becomes less important, and, although it still produces a fractional error of the same magnitude as the difference between K_1 and the true rCBV, this is the fractional error of the correction term, which is already a perturbation to the main effect.

Our correction algorithm, like the “baseline subtraction” method, assumes that in the absence of enhancement the tail of $S(t)$ returns to baseline. Those voxels for which the tail of $S(t)$ significantly rises above baseline noise are assumed to enhance and are excluded from the estimate of $\overline{\Delta R2}(t)$. It is conceivable that a small degree of agent extravasation could yield minute or undetectable enhancement that fails to meet our criteria for elevation of the tail of $S(t)$, but we postulate that in this circumstance the degree of T1 contamination would be negligible. It is also possible, however, that for profound signal intensity loss in cases of large blood volume contaminated $S(t)$ will still not have exceeded baseline by the end of dynamic imaging. A more inclusive method of identifying enhancing voxels would be to acquire delayed tail images several minutes after bolus administration rather than rely strictly on tail images at the end of the first pass. Alternatively, the conventional postcontrast T1-weighted images could conceivably be used as a mask.

We used a GE EPI acquisition in this study because it is sensitive to vessels of all sizes, as opposed to a SE acquisition, which has peak sensitivity to capillary-sized microvessels.³⁵ Although early reports documented significant correlation between SE rCBV and tumor grade,³⁶ this has been refuted subsequently by Donahue et al⁵ and Schmainda et al,³⁷ who demonstrated that GE- but not SE-derived rCBV maps significantly correlate with tumor grade. This would seem to underscore the fact that the neovascularity characteristic of aggressive, high-grade tumors often consists of disorganized, large-scale microvessels that do not have features typical of

capillaries^{38,39} and would therefore be best interrogated with GE acquisitions possessing wide-range microvascular sensitivity that can distinguish tumor angiogenesis from normal capillary beds. We maintain that GE acquisitions should be used for tumor perfusion studies because GE-based rCBV will be a statistically significant predictor of tumor grade. Of course, GE acquisitions are also sensitive to macrovessels, which must carefully be excluded from the regions of interest used to compute rCBV and estimate tumor grade. These macrovessels can be delineated by using guidance from postcontrast images or images with time-of-flight weighting.

The mean percentage differences between uncorrected and corrected rCBV were 2%, 16%, and 74% for grades II, III, and IV, respectively. This implies that, without leakage correction, estimated rCBV will on average be only little more than half of what it really should be for high-grade tumors and that leakage correction has no effect on the estimate in low-grade tumors. For a substantial number of cases (both low and high grade), corrected and uncorrected rCBV were identical, even for lesions with profound enhancement. We believe that this is because the predose of gadolinium, combined with what is presumably a low vascular permeability, effectively eliminated significant extravasation gradient over the time course of the bolus. Paradoxically low vascular permeability in high-grade tumors may be due to steroids, which were not accounted for in this study. The importance of the predose cannot be overemphasized⁵ and may be the difference between indiscernible signal intensity drop and a robust $\Delta R2(t)$ in very leaky tumors. The need for predose administration would theoretically be eliminated by using the double echo-correction technique, though a correction for the decrease in the susceptibility contrast effect due to presence of leaked gadolinium in the extravascular space still could artifactually decrease the estimated rCBV. The hypothesis that low vascular permeability accounts for the cases of minimal correction discrepancy could be tested by using techniques that estimate both rCBV and vascular permeability⁶ or vascular transfer constant.⁴⁰

We used the corrected rCBV maps in conjunction with the post-Gd T1-weighted images to select a necrosis-free region of interest for rCBV comparisons. This region of interest typically contained most if not all voxels with elevated rCBV in the tumor (“whole-tumor” region of interest selection), not just the maximum rCBV as has been proposed by several groups claiming significant correlation between rCBV and glioma grade (eg,^{1,2,4,41}). Because the rCBV maps were not used to guide biopsy, and it was not possible to correlate the rCBV maps with surgical specimens, this approach increased the chance that our region of interest included voxels that corresponded with the tissue used to establish the grade. An alternative approach would be to use a smaller region of interest that directly corresponds to the biopsy site or tissue from which the highest histopathologic grade was obtained, or from the small focus of highest rCBV on the blood volume maps (“hot-spot” region of interest selection). For the high-grade tumors with high vascular permeability, this alternative approach may yield even more disparity between corrected and uncorrected techniques, because the region of interest would not contain voxels with lower permeability to reduce differences in mean rCBV. Schmainda et al³⁷ demonstrated significant correlation between GE rCBV and glioma grade by using

both “whole-tumor” and “rCBV hot-spot” region of interest selection, so, for the GE technique, this aspect of region of interest selection should not impact our results. Nonetheless, future studies that deal with tumor heterogeneity, with and without correction techniques such as those described in this paper, are certainly in order.

The region of interest selection for tumor analysis is a controversial issue and the methods chosen for this work represent a practical and workable compromise. The use of enhancing areas on postcontrast T1-weighted images, though superficially attractive, is an imperfect solution for several reasons. Most notably, it is an indicator of blood-brain barrier permeability and not necessarily increased blood volume and may completely miss areas of high blood volume. Several studies have demonstrated a spatial mismatch between areas of increased blood volume and contrast enhancement (eg, ⁴²). Related to the issue of region of interest selection is the choice of reference region of interest. Whereas in this study we chose contralateral normal brain, other studies choose to normalize to uninvolved white matter. Initial studies (unpublished) indicate that this choice does not alter the overall conclusion of the study regarding the correlation of rCBV with tumor grade.

It is important to realize that, though corrected rCBV significantly correlates with tumor grade, which suggests that leakage correction is required for producing accurate estimates of rCBV, there exists substantial intragrade variability of rCBV (Fig 3B) that increases with tumor grade. This implies that, for a given corrected rCBV of an unknown lesion, tumor grade may not be assigned with a high degree of confidence, particularly when distinguishing between grades III and IV. This underscores the fact that glioma grading remains controversial⁴³ and multivariate and that factors in addition to blood volume (ie, vascular permeability, vessel size, rate of vessel proliferation and angiogenesis, and tumor metabolism) will probably be required to provide complete in vivo tumor assessment and prognosis.⁶ For example, a recent study³⁷ reported 96% and 69% accuracy when predicting high-grade and low-grade tumors, respectively, by using a combination of rCBV and a vessel size index derived from a combined GE/SE pulse sequence.

Conclusion

A robust strategy for approximately correcting the T1 enhancement contamination in DSC rCBV estimation is presented. This strategy uses linear fitting to estimate the T1 contamination caused by agent extravasation and, by removing the leakage term, allows generation of both corrected rCBV maps and first-order estimates of vascular permeability. We applied this technique to human brain tumor data, and our results show that Spearman rank correlation is significant between rCBV corrected for contrast agent extravasation and glioma grade, but not for uncorrected rCBV, primarily because of discrepancies for high-grade tumors that have greater blood-brain barrier disruption. This suggests that rCBV maps (and DSC perfusion parameter maps in general) should be computed with care. Otherwise, tumor grade may be underestimated, biopsy sites may be poorly selected, and response to therapy may be inaccurately assessed. Prebolus Gd probably plays a substantial role in reducing leakage contamination, and, despite significant correlation, there exists moderate cor-

rected rCBV variability within each tumor grade. This supports the notion that glioma grading remains controversial and that multiple parameters including vascular permeability and vessel size distribution will probably be required in aggregate for accurate prognostication.

Appendix

For susceptibility contrast imaging, the transverse relaxivity change ($\Delta R2^* = 1/T2^*$) in tissue with intact microvasculature is approximately proportional to the average contrast agent concentration in the capillaries $\overline{C_c}(t)$ times the vascular volume fraction (eg, ³⁵). Standard tracer kinetics (eg, ^{44,45}) relates $\overline{C_c}(t)$ to the convolution of the arterial input function, $C_a(t)$, with a capillary residue function, $R(t)$, which gives the fraction of input bolus remaining at time t :

$$A1) \quad \overline{C_c}(t) = F \cdot C_a(t) * R(t)$$

where F is the flow per unit volume. When there is no contrast extravasation, the integral of $\overline{C_c}(t)$ is proportional to the blood volume, because the central volume principle equates the time integral of $R(t)$ to V/F . Formally, this integration must be performed over all time, which can be approximated by using gamma fitting to extrapolate the tail of the first pass away from the recirculation peak.⁴⁶ As long as the arterial input function varies slowly and the integration is over a time that is substantially longer than the length of $R(t)$, however, any integral of Equation (A1) starting at $t = 0$ will be proportional to blood volume. If, however, the agent extravasates, the integral of Equation (A1) will no longer be proportional to the vascular volume fraction, but will reflect the (larger) volume of distribution of the agent.

For the derivations that follow, it is assumed that the leakage of contrast agent is a relatively small effect and is viewed as a perturbation over a time that is longer than the first pass of the agent, but short compared with its clearance time. Over this time scale (≤ 1 minute), we neglect back diffusion of agent from the extravascular to the intravascular space and can therefore represent the accumulation of agent in the tissue, C_T , as⁴⁷:

$$A2) \quad \frac{dC_T(t)}{dt} = PS \cdot \left(\overline{C_c}(t) - \frac{C_T(t)}{\lambda} \right) \approx PS \cdot \overline{C_c}(t) \rightarrow C_T(t) \approx PS \int_0^t \overline{C_c}(t') dt'$$

where PS is the product of permeability and surface area and λ is the partition coefficient between the extra- and intravascular space. C_T both decreases the intra- to extravascular susceptibility gradient, thereby decreasing susceptibility contrast, and also causes T1 relaxation enhancement within the extravascular space. Both effects reduce measured signal intensity changes and hence estimated blood volume.

As a starting approximation, we neglect the effect of C_T on the susceptibility contrast itself and focus on the (larger) T1 effects. For this, we assume that, when the contrast agent leaks into the interstitial space, water exchange between intracellular and extracellular spaces is fast^{48,49} and the blood volume is relatively small, so that extravasated agent simply decreases the

effective T1 of the tissue. As a result, the bolus of contrast agent causes a shift in T1 and T2*:

$$A3) \quad S(t) = M_0(1 - e^{-TR/T1} e^{-TR \cdot R1 \cdot C_T(t)}) e^{-TE/T2^*} e^{-TE \cdot \Delta R2^*(t)}$$

where R1 is the molar T1 relaxivity of the agent, $\Delta R2^*$ is the change in transverse relaxivity and is assumed to be proportional to the local fractional blood volume times $\overline{C_c}(t)$, and M_0 , T1, and T2* are the initial proton attenuation, longitudinal, and transverse relaxation times, respectively, for GE acquisitions. The corresponding baseline signal intensity, S_0 , is simply

$$A4) \quad S_0 = M_0(1 - e^{-TR/T1}) e^{-TE/T2^*}$$

Define:

$$A5) \quad \Delta \tilde{R}2^*(t) \equiv -\frac{\ln(S(t)/S_0)}{TE} = \Delta R2^*(t) - \frac{1}{TE} \ln \left[\frac{1 - e^{-TR/T1} e^{-TR \cdot R1 \cdot C_T(t)}}{1 - e^{-TR/T1}} \right]$$

where $\Delta \tilde{R}2^*$ is a contaminated estimate of $\Delta R2^*$ and is obtained by computing the ratio of $S(t)$ during the passage of agent with baseline S_0 . In the absence of T1 effects, $\Delta R2^*(t)$ plays the role of $\overline{C_c}(t)$ in Equation (A1), and thus would be integrated to form the relative blood volume estimate. For small T1-based enhancement (<30%, which is reasonable for typical TR and when a small initial loading dose of Gd-DTPA is applied), the $TR \cdot R1 \cdot C_T$ term is small, and $e^{-TR \cdot R1 \cdot C_T(t)}$ is thus approximately $1 - TR \cdot R1 \cdot C_T(t)$. Using the approximation $\ln(1 + \alpha/\beta) \approx \alpha/\beta$, where $\alpha = TR \cdot R1 \cdot C_T(t) \cdot e^{-TR/T1}$ and $\beta = 1 - e^{-TR/T1}$, Equation (A5) reduces to:

$$A6) \quad \Delta \tilde{R}2^*(t) \approx \Delta R2^*(t) - \frac{TR}{TE} \cdot \frac{e^{-TR/T1}}{1 - e^{-TR/T1}} \cdot R1 \cdot C_T(t).$$

Equation (A6) shows that the leakage attenuates the measured log signal intensity change by a term that is proportional to the tissue concentration of Gd-DTPA. If we had an estimate of C_T , we could subtract this term away and recover just the blood volume portion. Alternatively, if we had an accurate estimate of $\overline{C_c}(t)$ and PS we could use Equation (A2) to correct Equation (A6). As an approximation to this, we assume that the average of $\Delta R2^*(t)$ over parts of the brain without extravasation is proportional to $\overline{C_c}(t)$. Calling this average $\overline{\Delta R2^*(t)}$, we then have

$$A7) \quad \frac{dC_T(t)}{dt} = PS \cdot \overline{C_c}(t) = PS \cdot k \cdot \overline{\Delta R2^*(t)},$$

where k is an undetermined constant that depends on the average blood volume in the brain, vessel size, and other physiologic factors. If it is assumed that

$$A8) \quad \Delta R2^*(t) = K_1 \cdot \overline{\Delta R2^*(t)},$$

that is, the true $\Delta R2^*(t)$ for each pixel is a scaled version of the whole-brain $\overline{\Delta R2^*(t)}$, then for each pixel, $\Delta \tilde{R}2^*(t)$ can be expressed as a linear combination of T2*- and T1-dominated relaxivity terms, each of which is a function of $\overline{\Delta R2^*(t)}$:

$$A9) \quad \Delta \tilde{R}2^*(t) \approx K_1 \overline{\Delta R2^*(t)} - K_2 \int_0^t \overline{\Delta R2^*(t')} dt',$$

where

$$A10) \quad K_2 = \frac{TR}{TE} \cdot \frac{e^{-TR/T1}}{1 - e^{-TR/T1}} \cdot R1 \cdot k \cdot PS.$$

The right-hand-side of Equation (A9) has 2 unknowns, K_1 and K_2 , multiplying the (measured) brain-averaged log-signal change and its time integral. K_1 and K_2 can be determined by simple linear least-squares fitting, and then a corrected $\Delta \tilde{R}2^*(t)$ can be computed:

$$A11) \quad \Delta R2^*_{corr}(t) = \Delta \tilde{R}2^*(t) + K_2 \int_0^t \overline{\Delta R2^*(t')} dt'.$$

Finally, by integrating $\Delta R2^*_{corr}(t)$ we have a corrected estimate of the blood volume. In practice, because the time integral is the same for all pixels, this becomes a simple correction for each pixel that is proportional to the K_2 for that pixel:

$$A12) \quad rCBV_{corr} = rCBV + K_2 \int_0^T dt'' \int_0^{t''} \overline{\Delta R2^*(t')} dt',$$

where the double integral term is the same for all pixels, and T is the end time point for the numerical integration of the bolus.

Acknowledgments

We thank Dr. Scott D. Rand and Dr. Hendrikus G.J. Krouwer, from the Medical College of Wisconsin, for assistance in recruiting and running the patient studies, and Cathy Marszałkowski, Radiology Research Coordinator at the Medical College of Wisconsin, for coordinating the studies.

References

1. Sugahara T, Korogi Y, Kochi M, et al. **Perfusion-sensitive MR imaging of gliomas: comparison between gradient-echo and spin-echo echo-planar imaging techniques.** *AJNR Am J Neuroradiol* 2001;22:1306–15
2. Knopp EA, Cha S, Johnson G, et al. **Glial neoplasms: dynamic contrast-enhanced T2*-weighted MR imaging.** *Radiology* 1999;211:791–98
3. Lam WW, Chan KW, Wong WL, et al. **Pre-operative grading of intracranial glioma.** *Acta Radiol* 2001;42:548–54
4. Kremer S, Grand S, Remy C, et al. **Cerebral blood volume mapping by MR imaging in the initial evaluation of brain tumors.** *J Neuroradiol* 2002;29:105–13
5. Donahue KM, Krouwer HG, Rand SD, et al. **Utility of simultaneously acquired gradient-echo and spin-echo cerebral blood volume and morphology maps in brain tumor patients.** *Magn Reson Med* 2000;43:845–53
6. Law M, Yang S, Babb JS, et al. **Comparison of cerebral blood volume and vascular permeability from dynamic susceptibility contrast-enhanced perfusion MR imaging with glioma grade.** *AJNR Am J Neuroradiol* 2004;25:746–55
7. Lee SJ, Kim JH, Kim YM, et al. **Perfusion MR imaging in gliomas: comparison with histologic tumor grade.** *Korean J Radiol* 2001;2:1–7
8. Shin JH, Lee HK, Kwun BD, et al. **Using relative cerebral blood flow and volume to evaluate the histopathologic grade of cerebral gliomas: preliminary results.** *AJR Am J Roentgenol* 2002;179:783–89
9. Jackson A, Kassner A, Annesley-Williams D, et al. **Abnormalities in the recirculation phase of contrast agent bolus passage in cerebral gliomas: comparison with relative blood volume and tumor grade.** *AJNR Am J Neuroradiol* 2002;23:7–14
10. Roberts HC, Roberts TP, Bollen AW, et al. **Correlation of microvascular permeability derived from dynamic contrast-enhanced MR imaging with histologic grade and tumor labeling index: a study in human brain tumors.** *Acad Radiol* 2001;8:384–91

11. Tzika AA, Astrakas LG, Zarifi MK, et al. **Multiparametric MR assessment of pediatric brain tumors.** *Neuroradiology* 2003;45:1–10
12. Wu WC, Chen CY, Chung HW, et al. **Discrepant MR spectroscopic and perfusion imaging results in a case of malignant transformation of cerebral glioma.** *AJNR Am J Neuroradiol* 2002;23:1775–78
13. Aronen HJ, Pardo FS, Kennedy DN, et al. **High microvascular blood volume is associated with high glucose uptake and tumor angiogenesis in human gliomas.** *Clin Cancer Res* 2000;6:2189–200
14. Hartmann M, Heiland S, Harting I, et al. **Distinguishing of primary cerebral lymphoma from high-grade glioma with perfusion-weighted magnetic resonance imaging.** *Neurosci Lett* 2003;338:119–22
15. Kremer S, Grand S, Berger F, et al. **Dynamic contrast-enhanced MRI: differentiating melanoma and renal carcinoma metastases from high-grade astrocytomas and other metastases.** *Neuroradiology* 2003;45:44–49
16. Siegal T, Rubinstein R, Tzuk-Shina T, et al. **Utility of relative cerebral blood volume mapping derived from perfusion magnetic resonance imaging in the routine follow up of brain tumors.** *J Neurosurg* 1997;86:22–27
17. Cha S, Knopp EA, Johnson G, et al. **Dynamic contrast-enhanced T2-weighted MR imaging of recurrent malignant gliomas treated with thalidomide and carboplatin.** *AJNR Am J Neuroradiol* 2000;21:881–90
18. Fuss M, Wenz F, Essig M, et al. **Tumor angiogenesis of low-grade astrocytomas measured by dynamic susceptibility contrast-enhanced MRI (DSC-MRI) is predictive of local tumor control after radiation therapy.** *Int J Radiat Oncol Biol Phys* 2001;51:478–82
19. Burger PC, Vogel FS, Green SB, et al. **Glioblastoma multiforme and anaplastic astrocytoma: pathologic criteria and prognostic implications.** *Cancer* 1985;56:1106–11
20. Papadimitriou JM, Woods AE. **Structural and functional characteristics of the microcirculation in neoplasms.** *J Pathol* 1975;116:65–72
21. Hacklander T, Hofer M, Reichenbach J, et al. **[Possibilities of the use of MR tomography-based cerebral blood volume maps in the diagnosis of brain tumors].** *Rofo* 1995;163:484–89
22. Villringer A, Rosen BR, Belliveau JW, et al. **Dynamic imaging with lanthanide chelates in normal brain: contrast due to magnetic susceptibility effects.** *Magn Reson Med* 1988;6:164–74
23. Rosen BR, Belliveau JW, Vevea JM, et al. **Perfusion imaging with NMR contrast agents.** *Magn Reson Med* 1990;14:249–65
24. Boxerman JL, Rosen BR, Weisskoff RM. **Signal-to-noise analysis of cerebral blood volume maps from dynamic NMR imaging studies.** *J Magn Reson Imaging* 1997;7:528–37
25. Kleihues P, Burger PC, Scheithauer BW. **The new WHO classification of brain tumours.** *Brain Pathol* 1993;3:255–68
26. Weisskoff RM, Boxerman JL, Sorensen AG, et al. **Simultaneous blood volume and permeability mapping using a single Gd-based contrast injection.** In: *Proceedings of the Society of Magnetic Resonance, Second Annual Meeting*; 1994 Aug 6–12; San Francisco, Calif.; Berkeley, Calif: Society of Magnetic Resonance; 1994:279
27. Cox RW. **AFNI: software for analysis and visualization of functional magnetic resonance neuroimages.** *Comput Biomed Res* 1996;29:162–73
28. Cha S, Knopp EA, Johnson G, et al. **Intracranial mass lesions: dynamic contrast-enhanced susceptibility-weighted echo-planar perfusion MR imaging.** *Radiology* 2002;223:11–29
29. Wong JC, Provenzale JM, Petrella JR. **Perfusion MR imaging of brain neoplasms.** *AJR Am J Roentgenol* 2000;174:1147–57
30. Wetzel SG, Cha S, Johnson G, et al. **Relative cerebral blood volume measurements in intracranial mass lesions: interobserver and intraobserver reproducibility study.** *Radiology* 2002;224:797–803
31. Vonken EJ, van Osch MJ, Bakker CJ, et al. **Measurement of cerebral perfusion with dual-echo multi-slice quantitative dynamic susceptibility contrast MRI.** *J Magn Reson Imaging* 1999;10:109–17
32. Vonken EP, van Osch MJ, Bakker CJ, et al. **Simultaneous quantitative cerebral perfusion and Gd-DTPA extravasation measurement with dual-echo dynamic susceptibility contrast MRI.** *Magn Reson Med* 2000;43:820–27
33. Uematsu H, Maeda M, Sadato N, et al. **Blood volume of gliomas determined by double-echo dynamic perfusion-weighted MR imaging: a preliminary study.** *AJNR Am J Neuroradiol* 2001;22:1915–19
34. Enochs WS, Harsh G, Hochberg F, et al. **Improved delineation of human brain tumors on MR images using a long-circulating, superparamagnetic iron oxide agent.** *J Magn Reson Imaging* 1999;9:228–32
35. Boxerman JL, Hamberg LM, Rosen BR, et al. **MR contrast due to intravascular magnetic susceptibility perturbations.** *Magn Reson Med* 1995;34:555–66
36. Aronen HJ, Gazit IE, Louis DN, et al. **Cerebral blood volume maps of gliomas: comparison with tumor grade and histologic findings.** *Radiology* 1994;191:41–51
37. Schmainda KM, Rand SD, Joseph AM, et al. **Characterization of a first-pass gradient-echo spin-echo method to predict brain tumor grade and angiogenesis.** *AJNR Am J Neuroradiol* 2004;25:1524–32
38. Deane BR, Lantos PL. **The vasculature of experimental brain tumours. Part 1. A sequential light and electron microscope study of angiogenesis.** *J Neurol Sci* 1981;49:55–66
39. Zama A, Tamura M, Inoue HK. **Three-dimensional observations on microvascular growth in rat glioma using a vascular casting method.** *J Cancer Res Clin Oncol* 1991;117:396–402
40. Johnson G, Wetzel SG, Cha S, et al. **Measuring blood volume and vascular transfer constant from dynamic, T₂*-weighted contrast-enhanced MRI.** *Magn Reson Med* 2004;51:961–68
41. Yang D, Korogi Y, Sugahara T, et al. **Cerebral gliomas: prospective comparison of multivoxel 2D chemical-shift imaging proton MR spectroscopy, echoplanar perfusion and diffusion-weighted MRI.** *Neuroradiology* 2002;44:656–66
42. Wagner ML, Ulmer JL, Rand SD, et al. **Relationship between contrast enhancement and brain tumor neovascularity revealed by blood volume functional imaging.** In: *ASNR American Society of Neuroradiology 42nd Annual Meeting*; 2004 Jun 5–11; Seattle, Wash; Oak Brook, Ill: American Society of Neuroradiology; 2004:18
43. Dumas-Duport C, Scheithauer B, O'Fallon J, et al. **Grading of astrocytomas. A simple and reproducible method.** *Cancer* 1988;62:2152–65
44. Lassen NA. **Cerebral transit of an intravascular tracer may allow measurement of regional blood volume but not regional blood flow.** *J Cereb Blood Flow Metab* 1984;4:633–34
45. Weisskoff RM, Chesler D, Boxerman JL, et al. **Pitfalls in MR measurement of tissue blood flow with intravascular tracers: which mean transit time?** *Magn Reson Med* 1993;29:553–58
46. Thompson H, Starmer C, Whalen R, et al. **Indicator transit time considered as a gamma variate.** *Circ Res* 1964;14:502–15
47. Larsson H, Stubgaard M, Frederiksen J, et al. **Quantitation of blood-brain barrier defect by magnetic resonance imaging and gadolinium-DTPA in patients with multiple sclerosis and brain tumors.** *Magn Reson Med* 1990;16:117–31
48. Donahue KM, Burstein D, Manning WJ, et al. **Studies of Gd-DTPA relaxivity and proton exchange rates in tissue.** *Magn Reson Med* 1994;32:66–76
49. Quirk JD, Bretthorst GL, Duong TQ, et al. **Equilibrium water exchange between the intra- and extracellular spaces of mammalian brain.** *Magn Reson Med* 2003;50:493–99